Selective measurement of hole tunneling times through AlGaAs barriers based on the quantum confined Stark effect

N. Le Thomas
Département de Recherche Fondamentale sur la Matière Condensée, CEA/Grenoble, 38054 Grenoble Cedex 9, France

N. T. Pelekanos
Microelectronics Research Group, FORTH/IESL, P.O. Box 1527, 71110 Heraklion, Greece
and Materials Science and Technology Department, University of Crete, P.O. Box 2208, 71003 Heraklion, Greece

Z. Hatzopoulos
Microelectronics Research Group, FORTH/IESL, P.O. Box 1527, 71110 Heraklion, Greece
and Physics Department, University of Crete, P.O. Box 2208, 71003 Heraklion, Greece
(Received 31 May 2005; revised manuscript received 3 November 2005; published 19 December 2005)

We demonstrate a method able to measure selectively and over a wide dynamic range the tunneling time of electrons or holes through a given potential barrier in a semiconductor heterostructure. The method relies on appropriate band gap engineering of the intrinsic region of a *p-i-n* diode, and on the quantum confined Stark effect. As an example, the hole tunneling time through thick $Al_xGa_{1-x}As$ potential barriers has been measured over six orders of magnitude in InGaAs/AlGaAs structures. For $x=0.6$, ultralong hole tunneling times are demonstrated in fair agreement with a semiclassical tunneling model. This model however turns out to be inapplicable for $x \leqslant 0.4$, overestimating the tunneling times by several orders of magnitude. This suggests the formation of intrinsic leakage current paths through the AlGaAs barriers at these concentrations.

DOI: 10.1103/PhysRevB.72.235323 PACS number(s): 73.40.Gk, 73.40.Lq

Carrier tunneling through a potential barrier is perhaps the most fundamental quantum-mechanical process, with direct applications in numerous semiconductor devices, such as, for instance, resonant tunneling diodes,[1,2] single-electron transistors,[3] quantum cascade lasers,[4] or tunable lasers.[5] Considering that tunneling depends critically on a number of heterostructure parameters, which are usually imperfectly known, it is often necessary to recourse to experiment in order to estimate *accurately* the actual tunneling time in a given heterostructure. There are two basic approaches to extract carrier tunneling times in semiconductor heterostructures. The first is by analyzing the static current-voltage characteristics of single or double barrier heterostructures.[6] A technical difficulty in this approach is that the "tunneling" current should be dominant over all other possible current contributions. Moreover, the analysis relies also on good knowledge of heterostructure parameters and a number of idealizations to take into account the variable bias conditions in the heterostructure. Therefore, the extracted carrier tunneling information in this approach can only be regarded as very approximative.

The second more direct approach to measure tunneling times in semiconductor heterostructures is by time resolved photoluminescence (PL) experiments.[7,8] In this approach, electrons and holes are optically injected in a given quantum well (QW) of the heterostructure. If the carriers tunnel out of the QW in a time scale that is comparable or smaller than the recombination time, then the QW PL decay time is significantly shortened and an effective carrier tunneling time τ_{tun} can be readily deduced. Obviously, the tunneling times that can be measured cannot be longer than the recombination time, which in typical semiconductor heterostructures is of the order of nanoseconds. This practically limits the approach to structures with relatively "transparent" barriers, and the extracted tunneling times cannot span over a very large dynamic range. Another serious concern in the approach is that τ_{tun} contains contributions from both electron and hole tunneling events, implying that in order to draw conclusions on the tunneling dynamics of one type of carrier several approximations have to be made.

In the following, we propose a simple method to extract selectively and over a wide dynamic range the electron or hole tunneling time through a given potential barrier. It is based on a proper band gap engineering of the active region of a *p-i-n* diode and consists essentially of recording the current I_0 for which the optical emission spectrum of a probe QW starts shifting due to the quantum confined Stark effect (QCSE). We illustrate this method for hole tunneling through $Al_xGa_{1-x}As$ barriers of different widths and compositions, which are incorporated in the intrinsic region of a *p-i-n* diode.

In Fig. 1(a) the proposed band gap lineup to measure the barrier transparency in relation to holes is presented. The structure consists of the barrier under test, a wide probe QW whose lowest transition is the ground state of the whole structure, and a collection quantum well (CQW) used to collect the "tunneling" carriers. Due to the bipolar nature of carrier injection, these two QWs accumulate in steady-state forward bias conditions a charge density $-qN$ of electrons and $+qN$ of holes on either side of the barrier. In the low-injection regime, if J is the injected current density and τ the carrier transfer time through the barrier, then

$$N = \frac{\tau J}{q}. \tag{1}$$

This produces a current-dependent space-charge field which peaks at the barrier and extends significantly inside the QWs

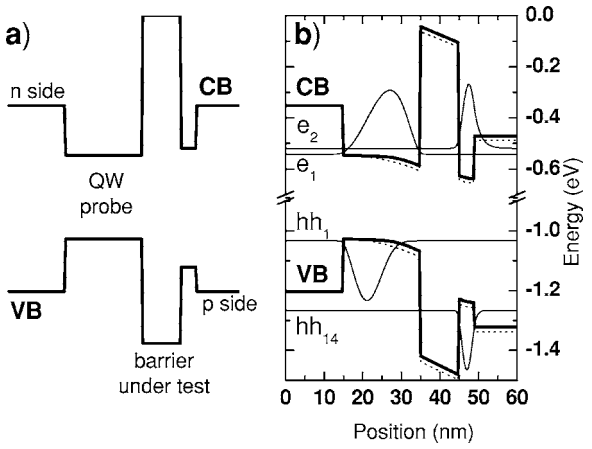

FIG. 1. (a) Band diagram schematic of the proposed structure to measure the barrier tunneling time. (b) Typical computed band bending of the conduction and valence bands for $I=15$ mA and $\tau_{hh}=30$ ns with (solid line) and without (dot line) field screening. For the former case, the two first electron wave functions of the structure under carrier injection as well as the first and 14th heavy hole wave functions are also shown.

tuning their emission by QCSE. The field's maximum value is

$$F = \frac{qN}{\epsilon} = \frac{\tau J}{\epsilon}, \tag{2}$$

where ϵ the material permittivity. For a homogeneously applied electric field F, the corresponding redshift of the QW electroluminescence (EL) can be expressed as

$$\Delta\lambda = \alpha F^2. \tag{3}$$

The α parameter depends on the QW width: $\alpha \sim 1.4 \times 10^{-3}$ nm/(kV/cm)^2, for a 10 nm QW if $F < 60$ kV/cm and $\alpha \sim 12.5 \times 10^{-3}$ nm/(kV/cm)^2, for a 20 nm QW if $F < 40$ kV/cm. To account for the fact that the space-charge field mainly acts on the barrier and spreads over only about half of the QW width, for a 20 nm QW we choose $\alpha \sim 1.4 \times 10^{-3}$ nm/(kV/cm)^2. Due to the quadratic dependence of $\Delta\lambda$ versus F and therefore versus J, an abrupt onset of $\Delta\lambda$ can be observed in the emission wavelength-current characteristic, as soon as N becomes of the order of 10^{11} cm^{-2}. Defining as J_0 the current density needed to achieve $\Delta\lambda = 0.5$ nm, we can obtain by combining Eqs. (1)–(3) a simple formula to estimate the transfer time:

$$\tau = \frac{\epsilon}{J_0}\sqrt{\frac{0.5nm}{\alpha}}. \tag{4}$$

The current-wavelength characteristic gives thus simple access to the carrier transfer time. In the following, we measure at the onset of $\Delta\lambda$ the corresponding current $I_0 = J_0 S$ with S being the surface of the contact, and use Eq. (4) to obtain an estimate of $Al_xGa_{1-x}As$ barriers' transparency.

With the band diagram proposed in Fig. 1 only the probe QW exhibits spontaneous emission for reasonable space-charge fields. Indeed electrons that are captured in this QW do not have enough energy to escape toward the CQW until the fundamental electron levels of these two QWs, which are the two fundamental electron levels of the whole structure, align. Their associated wave functions labeled e_1 and e_2, as well as their relative energy positions are computed in Fig. 1(b) in a typical case. It follows that only holes can accumulate in the CQW in the low current regime. On the contrary, the holes can be injected inside the probe QW via tunneling from the CQW with a rate that depends on the barrier transparency. As only the probe QW can emit light in the low current regime of interest here, it will be named hereafter as the active QW (AQW). It should be noted that the configuration in Fig. 1(a) allows us to record only hole tunneling times, nevertheless to have access to the electron tunneling times one needs merely to invert the n- and p-side regions.

To test this method InGaAs/AlGaAs light-emitting diodes (LEDs) have been fabricated by molecular beam epitaxy on (100) GaAs n^+ substrates. In all the samples, the structure shown in Fig. 1(a) is located at the center of a 300 nm undoped $Al_{0.2}Ga_{0.8}As$ SCH region, and the p-i-n diode is formed by 1.6 μm thick $Al_{0.3}Ga_{0.7}As$ cladding layers, Si doped for the N side and Be doped for the P side. The tunneling barrier under test is made of $Al_xGa_{1-x}As$ with x varying between 0.3 and 0.6 and a width between 5 and 10 nm. In most samples, the AQW was chosen to be a 20 nm wide $In_{0.1}Ga_{0.9}As$ layer, to fully exploit QCSE. In the case of samples 6 and 7, where the AQW consisted of $In_{0.2}Ga_{0.8}As$, the AQW width was limited to 10 nm in order to stay below critical thickness. The CQW is a 6 nm wide InGaAs QW for all samples except for samples 1 and 2 where it is 11 nm wide, allowing in both cases an efficient collection of holes. In Table I, we summarize for all samples their main structural parameters, as well as the measured I_0 values and experimentally deduced hole tunneling times.

In Figs. 2(a) and 2(b) we show the $T=10$ K surface-detected EL spectra of the AQW as a function of current for samples 3 and 4. As can be seen in Table I, these samples differ only in the barrier width and height, whereas all other structural parameters are identical. The dashed spectra depict in each case the 20 nm AQW photoluminescence (PL) peak obtained in flat band conditions (i.e., having confirmed that the diode field is screened out). For low currents ($I < I_0$), the AQW EL and PL peaks coincide, implying that no significant space-charge field exists in the structure. For $I \simeq I_0$, the accumulated space charge becomes sufficient to start shifting the AQW EL peaks according to QCSE. From the shift onset in the spectra, one can determine that $I_0 \simeq 0.25$ mA for sample 3 and $I_0 \simeq 0.01$ μA for sample 4. This striking difference (more than three decades) suggests a strong effect resulting from the $Al_xGa_{1-x}As$ tunneling barrier.

In Fig. 3(a) the wavelength shift $\Delta\lambda$ versus current are plotted for several of our samples, including a reference one consisting of a single 20 nm AQW inside the intrinsic region. A distinct shift onset is clearly observed for all samples, except for the reference one as expected. The current I_0 for which $\Delta\lambda \sim 0.5$ nm is marked by an arrow labeled with the sample number. Figure 3(a) clearly reveals that I_0 depends on the barrier parameters and follows some special trends. Indeed when the barrier thickness increases, I_0 decreases as shown with the samples series (1, 2, 3) or (4, 5). When the Al content inside the barrier drops, I_0 increases as shown by

TABLE I. Sample parameters: L_b is the barrier thickness, x_{Al} the barrier aluminium concentration, $x1_{\mathrm{In}}$, and $x2_{\mathrm{In}}$ the indium concentrations in the AQW and CQW, respectively, L_{AQW} the AQW thickness, L_p the CQW thickness, I_0 the current at the onset of $\Delta\lambda$, $\tau 1_{hh}$ the hole tunneling time obtained with Eq. (4), and $\tau 2_{hh}$ the one extracted from a more developed model including screening (see text).

Sample name	L_b (nm)	x_{Al} (%)	L_{AQW} (nm)	$x1_{\mathrm{In}}$ (%)	L_p (nm)	$x2_{\mathrm{In}}$ (%)	I_0 (mA)	$\tau 1_{hh}$ (ns)	$\tau 2_{hh}$ (ns)
1	6	30	20	10	11	0	20	7	9.1
2	8	30	20	10	11	0	1	130	50
3	10	30	20	10	6	0	0.25	520	215
4	6.6	60	20	10	6	0	$2\cdot10^{-5}$	$6.5\cdot10^{6}$	$5\cdot10^{6}$
5	5	60	20	10	6	0	$4\cdot10^{-3}$	$3.3\cdot10^{4}$	$3\cdot10^{4}$
6	10	40	10	20	6	0	0.1	$2.8\cdot10^{3}$	$3\cdot10^{3}$
7	10	30	10	20	6	0	1	280	230
8	8.8	30	20	10	6	10	0.2	650	300
9	11	30	20	10	6	10	0.07	$1.9\cdot10^{3}$	$2\cdot10^{3}$

samples 6 and 7. Such behavior is qualitatively consistent with the semiclassical picture of the tunneling effect[9] where the transit time of the carrier inside the CQW, which we call here tunneling time τ_{hh}, is given by:

$$\tau_{hh} \approx L_p \sqrt{\frac{2m_p}{e_h}} \exp\left(2L_b \sqrt{\frac{2m_b(\Delta_h - e_h)}{\hbar^2}}\right), \qquad (5)$$

with L_p and L_b the CQW and barrier width, m_p and m_b the heavy hole effective masses in these layers, respectively, e_h the heavy hole energy confined level in the CQW, and Δ_h the potential offset between the barrier and the CQW. Finally, comparing samples 3 and 7 which differ only in the AQW width, we observe a much steeper current dependence of $\Delta\lambda$ for sample 3 in accordance to QCSE.

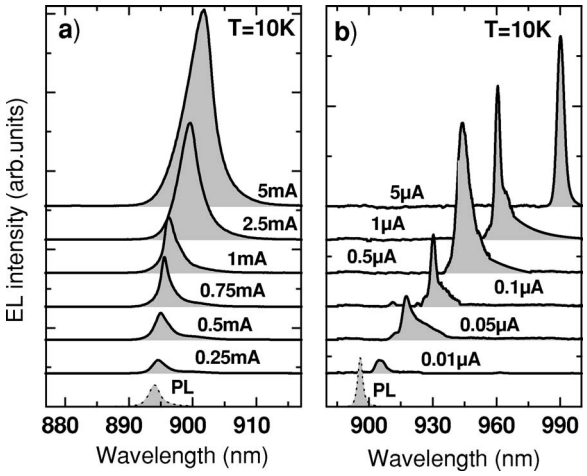

FIG. 2. EL spectra with increasing dc injection current from the AQW of (a) sample 3 and (b) sample 4. The dashed curves denote the corresponding PL spectra. The samples were processed in 300 μm wide mesas to minimize lateral carrier recombination effects and 2 mm long cavities. A semitransparent Pt top contact allowed surface detection of EL. The LEDs were welded with indium on gold ceramic (Al_2O_3) and were mounted in a helium flow cryostat. The carriers were injected with a KEITHLEY 220 current source.

For currents higher than I_0, discontinuities appear in the wavelength shift for some of the samples, such as, for instance, samples 2 and 3. As explained in Ref. 10, this is attributed to a sudden electron leakage from the AQW toward the CQW, which is made possible when the space-charge field becomes sufficiently strong to align the fundamental electron levels e_1 and e_2 in the two QWs. This interpretation is supported by the sudden appearance at the discontinuity current of strong EL from the CQW, not shown in Fig. 2, indicating that electrons actually make it to CQW.

In Table I, we report the heavy hole tunneling time $\tau 1_{hh}$ estimated from I_0 and Eq. (4). We also deduced $\tau 2_{hh}$ with a more advanced model, whose main lines are as follows: For

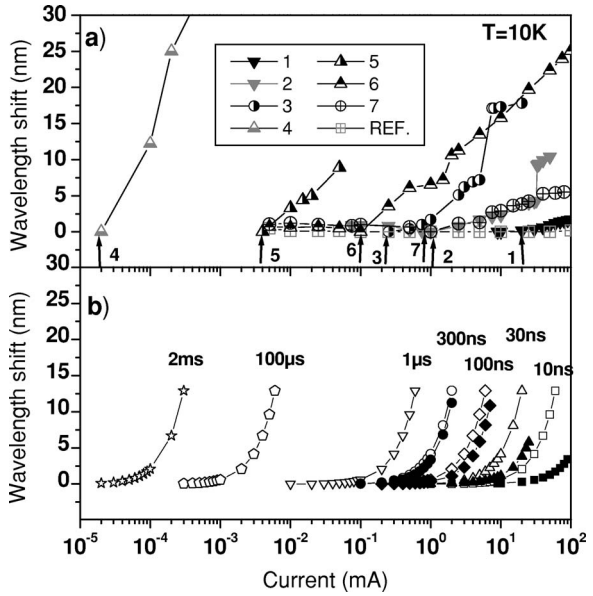

FIG. 3. (a) Experimental $\Delta\lambda$ as a function of injection current, observed by EL at 10 K for several diodes with different tunneling barriers (cf. Table I). (b) Theoretical $\Delta\lambda$ versus current curves for a 20 nm AQW and different heavy hole tunneling times τ_{hh}, with (solid symbols, where shown) or without (open symbols) taking into account carrier screening inside the AQW. Screening effects in the 20 nm AQW decrease substantially $\Delta\lambda$ for $\tau_{hh} < 100$ ns.

a given injection current, we solve the system of rate equations for the steady state carrier densities inside the AQW and the CQW, using the hole transfer time τ_{hh} as the input parameter. We assume that the holes enter into AQW by tunneling from the CQW, neglecting thermionic emission and overshooting of carriers over the barriers. Also, until the fundamental electron levels e_1 and e_2 in the two QWs align, electrons are present only in AQW. Furthermore, we assume that the carriers recombine in AQW with a bimolecular recombination rate of 10^{10} cm^3/s. Once the carrier distribution in the QWs is known, we obtain the charge density by weighting with the corresponding envelope functions, and solve Poisson's equation by a relaxation method[11] to determine the new energy band profile. With the new profile, we solve again Schrödinger's equation by the finite element method, and the procedure is iterated until a satisfactory convergence for $\Delta\lambda$ is reached. By comparing the calculated with the experimental onset of $\Delta\lambda$, we adjust accordingly τ_{hh} until good agreement is achieved.

The main difference between the two models is that in the second model $\Delta\lambda$ is computed from the exact carrier-modified band gap lineup of the structure, instead of the phenomenological Eq. (3) of the first model, where an effective AQW width is appropriately chosen. This clearly should result to a refinement of the extracted τ_{hh} values. Even though the second model goes well beyond the first one, it still uses several approximations. For instance, it does not take into account the gradual decrease of τ_{hh} as the CQW gets increasingly filled and the barrier is more bent. Our calculations, however, show that this effect becomes important only at strong charging situations, i.e., for currents much higher than I_0 where the onset of $\Delta\lambda$ occurs. In addition, the model neglects any Pauli exclusion effects for the hole tunneling event, which is justified by the large energy difference in our samples between the hole fundamental levels in the two QWs (cf. Fig. 1).

In Fig. 3(b) we plot the calculated $\Delta\lambda(I)$ curves obtained by the second model for a 20 nm AQW and for different τ_{hh} values. In each curve, the shift is computed until e_1 and e_2 align. In Fig. 1(b), we show for $I=15$ mA the band-profile outcome of the self-consistent solution of Schrödinger-Poisson equations, which is necessary in order to take into account screening effects of opposite charge carriers inside the AQW. As can be seen by the solid symbol curves in Fig. 3(b), screening effects result in a slowing down of $\Delta\lambda$ for $\tau_{hh}<300$ ns. By fitting the experimental $\Delta\lambda(I)$ curves of Fig. 3(a) with theoretical curves such as the ones shown in Fig. 3(b), we deduce the $\tau 2_{hh}$ values of Table I.

The fitting procedure is illustrated in Fig. 4, where we plot for samples 3 and 1 the experimental $\Delta\lambda(I)$ points and compare them with best fitting curves from second model. We observe that for $\Delta\lambda<2$ nm, which is the region of interest in this work, the experimental points are well reproduced by the theoretical curves. On the other hand, for $\Delta\lambda>2$ nm we clearly observe a saturation behavior in both samples, which can be attributed as already mentioned to a gradual increase of barrier transparency by the combined effects of carrier band filling in the CQW and space-charge-induced bending of the tunneling barrier. For the specific samples of Fig. 4, we deduce $\tau 2_{hh}=(9.1\pm0.5)$ ns and $\tau 2_{hh}=(215\pm15)$ ns for

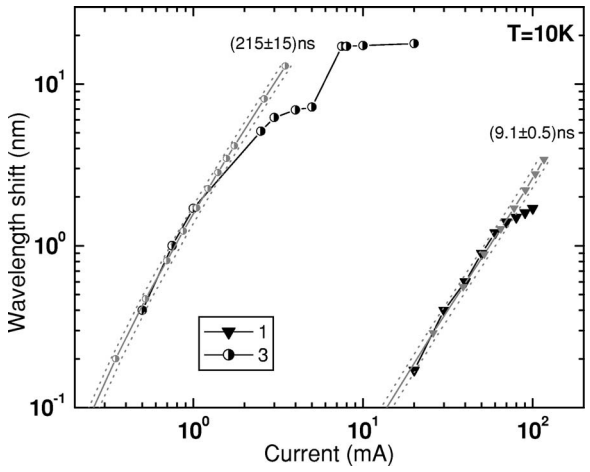

FIG. 4. Experimental $\Delta\lambda$ versus current data points (dark and big symbols) observed by EL at 10 K for samples 1 and 3, compared to the corresponding modeling curves (gray and small symbols) calculated for a 20 nm AQW and variable τ_{hh}. In each case the dot lines give the incertitude interval.

samples 1 and 3, respectively. It is interesting to note, however, that the extracted $\tau 1_{hh}$ and $\tau 2_{hh}$ values in Table I are very similar. This implies that the simple Eq. (4) is sufficient to give a quick estimate to the tunneling time through potential barriers.

Although the semiclassical model reproduces some of the trends of the hole tunneling times deduced from I_0 in regard to barrier thickness and height, it certainly fails to fit them quantitatively. In Fig. 5, the experimental tunneling times (open symbols) and the theoretical ones (dashed line) are plotted as a function of the dimensionless quantity $L_b\sqrt{m_b(\Delta_h-e_h)/\hbar^2}$ in order to account for the different barrier parameters between samples. For samples 5 and 4, with $x=0.6$, we observe very long tunneling times of 30 μs and

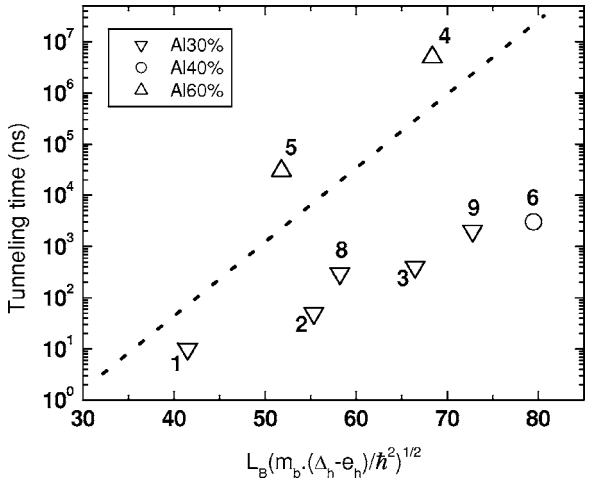

FIG. 5. Comparison between theoretical (dashed line) and experimental (open symbols) heavy hole tunneling times versus $L_b\sqrt{m_b(\Delta_h-e_h)/\hbar^2}$ for all samples. The theoretical curve results from the semiclassical tunneling model. The samples are grouped and denoted by a different symbol according to their aluminium concentration in the barrier.

5 ms, respectively, which are distinctly higher than what expected by the semiclassical model. This can be explained by the fact that in these samples where I_0 is small, the experimental tunneling times may be overestimated due to current inhomogeneities over the wide (2 mm $\times$ 300 μm) current injection area. In contrast, for $x=0.3$ and $x=0.4$, the experimental tunneling times are orders of magnitude below the expected theoretical times, with values ranging from 10 ns to 1 μs. In the following, we discuss this unexpected discrepancy.

Previous studies on tunnel transfer time were mainly focused on carrier transfer through thin barriers (<5 nm). They revealed most of the times a good agreement with the semiclassical model.[9,12] Departure from this model was generally attributed to resonant tunneling[13,15] or band mixing effects in the case of hole tunneling.[14,16] Such effects, however, are expected to be negligible in our thick barrier samples.

Later on, interest for thick tunneling barriers (>10 nm) appeared. From PL and PL excitation on asymmetrical GaAs/AlGaAs QW, Tomita *et al.*[17] demonstrated a very efficient carrier transfer through $Al_{0.3}Ga_{0.7}As$ barriers with thicknesses varying between 10 and 30 nm. As in our case, they observed a relatively weak dependence on the barrier thickness compared to the semiclassical model. To explain their results, they proposed an excitonic transfer from one well to the other via dipole-dipole interaction. Here this explanation is not relevant because of the lack of excitons in the CQW. For the same reason, the theory proposed by Lyo[18] relying on photon exchange can be ignored. In Ref. 19, an unexpected carrier transfer through a 52 nm thick $Cd_{0.18}Zn_{0.82}Te$ barrier was also found. The fact that the barrier is an alloy seems to be an important characteristic to explain the observed efficient transfer through thick barriers. Kim *et al.*[20] also measured optically a strong leakage through $Al_xGa_{1-x}As$ barriers with $x \leqslant 0.35$ and thickness between 30 and 150 nm, while for AlAs or GaAs barriers the effect vanished. They suggested an intrinsic inhomogeneity mechanism in the alloy barrier. With a three-dimensional quantum-mechanical calculation the observed phenomena were explained by supposing a microscopic clustering (around 20–30 Å in size) of GaAs in a quantum-wire-like fashion inside the alloy barrier. For $x>0.5$ a clustering of 20–30 Å is not enough to create a sufficient number of low potential pathways. Their model seems in line with our measurements which exhibit efficient transfer for $x \leqslant 0.4$ and the contrary for $x=0.6$.

In summary, we have proposed a method based on the quantum confined Stark effect, capable of measuring selectively and in a large dynamic range the carrier transfer time through tunneling barriers in bipolar devices under operating conditions. By applying it to $Al_xGa_{1-x}As$ barriers, hole tunneling times as large as 5 ms have been recorded for x $=0.6$. Moreover, in agreement with previous studies, we have shown that for $x \leqslant 0.4$, the hole transfer through the barrier becomes unexpectedly fast.

We thank the Laboratoire Infrarouge of CEA/Grenoble for free access to its processing facility. This work has been partially supported by the European Project No. IST-FET-31028.

[1] L. L. Chang, L. Esaki, and R. Tsu, Appl. Phys. Lett. **24**, 593 (1974).
[2] J. C. Blakesley, P. See, A. J. Shields, B. E. Kardynal, P. Atkinson, I. Farrer, and D. A. Ritchie, Phys. Rev. Lett. **94**, 067401 (2005).
[3] David M.-T. Kuo and Y.-C. Chang, Phys. Rev. B **72**, 085334 (2005).
[4] J. Faist, F. Capasso, D. L. Sivco, C. Sirtori, A. L. Hutchinson, and A. Y. Cho, Science **264**, 553 (1994).
[5] N. Le Thomas, N. T. Pelekanos, and Z. Hatzopoulos, Appl. Phys. Lett. **83**, 1304 (2003).
[6] M. Tsuchiya and H. Sakaki, Jpn. J. Appl. Phys., Part 2 **25**, L185 (1986).
[7] M. Tsuchiya, T. Matsusue, and H. Sakaki, Phys. Rev. Lett. **59**, 2356 (1987).
[8] M. Nido, M. G. W. Alexander, W. W. Rühle, T. Schweizer, and K. Köhler, Appl. Phys. Lett. **56**, 355 (1990).
[9] W. W. Rühle, A. P. Heberle, M. G. W. Alexander, M. Nido, and K. Köhler, Phys. Scr., T **39**, 278 (1991).
[10] N. Le Thomas, N. T. Pelekanos, Z. Hatzopoulos, E. Aperathitis, and R. Hamelin, Appl. Phys. Lett. **81**, 1582 (2002).
[11] C. M. Weinert and N. Agrawal, J. Appl. Phys. **76**, 7947 (1994).
[12] B. Deveaud, A. Chomette, F. Clerot, P. Auvray, A. Regreny, R. Ferreira, and G. Bastard, Phys. Rev. B **42**, 7021 (1990).
[13] M. G. W. Alexander, M. Nido, W. W. Rühle, and K. Köhler, Phys. Rev. B **41**, 12295 (1990).
[14] R. Ferreira and G. Bastard, Rep. Prog. Phys. **60**, 345 (1997).
[15] D. Y. Oberli, J. Shah, T. C. Damen, C. W. Tu, T. Y. Chang, D. A. B. Miller, J. E. Henry, R. F. Kopf, N. Sauer, and A. E. DiGiovanni, Phys. Rev. B **40**, 3028 (1989).
[16] M. F. Krol, S. Ten, B. P. McGinnis, M. J. Hayduk, G. Khitrova, and N. Peyghambarian, Phys. Rev. B **52**, 14344 (1995).
[17] A. Tomita, J. Shah, and R. S. Knox, Phys. Rev. B **53**, 10793 (1996).
[18] S. K. Lyo, Phys. Rev. B **62**, 13641 (2000).
[19] S. Haacke, N. T. Pelekanos, H. Mariette, M. Zigone, A. P. Heberle, and W. W. Rühle, Phys. Rev. B **47**, 16643 (1993).
[20] D. S. Kim, H. S. Ko, Y. M. Kim, S. J. Rhee, S. C. Hohng, Y. H. Yee, W. S. Kim, J. C. Woo, H. J. Choi, J. Ihm, D. H. Woo, and K. N. Kang, Phys. Rev. B **54**, 14580 (1996).